BULETINUL INSTITUTULUI POLITEHNIC DIN IAŞI
Publicat de
Universitatea Tehnică „Gheorghe Asachi” din Iaşi
Volumul 69 (73), Numărul 2, 2023
Secţia
ELECTROTEHNICĂ. ENERGETICĂ. ELECTRONICĂ
DOI:10.2478/bipie-2023-0010

STUDY OF HEAT TRANSFER AND FLOW MECHANISM IN CIRCULAR BACKWARD-FACING STEP CONSIDERING FERROFLUID FLOW UNDER MAGNETIC FIELD EFFECT

BY

EMREHAN GÜRSOY[1,*] and ENGİN GEDİK[2]

[1]Institute of Graduate Programs, Energy Systems Engineering, Karabük University, Karabük, Türkiye
[2]Faculty of Engineering, Mechanical Engineering, Karabük University, Karabük, Türkiye

Received: June 14, 2024
Accepted for publication: July 28, 2024

Abstract. The backward-facing step is critical in heat transfer applications, especially in heating and cooling systems, due to its unique flow phenomena like reattachment and separation. Expansion ratio, angle, flow regime, and thermo-physical properties of the working fluid significantly impact heat transfer and flow mechanisms. In the present work a numerical study was conducted on circular cross-section backward-facing step with 2.5 expansion ratio and 90° angle. Magnetizable ferrofluid with volume concentrations of φ=1.0, 1.5, and 2.0% were used in laminar flow regimes ($500 \leq Re \leq 2000$), exposed to a constant magnetic field (B=0.3, 0.5, 0.7, and 1.0T) and a constant heat flux ($q''=600\ W/m^2$). Results showed that φ=1.0% ferrofluid had the highest Nusselt number and performance evaluation criterion. Besides, the increment of magnetic field strength not only enhances convective heat transfer but also causes its reduction. The magnetic field significantly influenced reattachment and recirculation, and the optimum case is acquired in B=0.5T at Re=500.

---

*Corresponding author; *e-mail*: emrehangursoy@gmail.com

Keywords: Backward facing step, laminar flow regime, ferrofluid, DC magnetic field, performance evaluation criterion.

1. Introduction

In engineering applications, backward-facing step (BFS) geometry has a remarkable importance due to the fact that it is combined with many flow phenomena such as reattachment and separation (Chen *et al*., 2018). Furthermore, the stream in BFS is investigated into four sections as can be seen in Fig. 1: reattachment region, recirculation region, attached region, and separated shear layer (Guo *et al*., 2017). BFS is used in many industries and engineering areas such as heat transfer, chemical process, electronic sector, and cooling of turbine blades as internal flow applications while it has been utilized in external flow applications such as in aircraft.

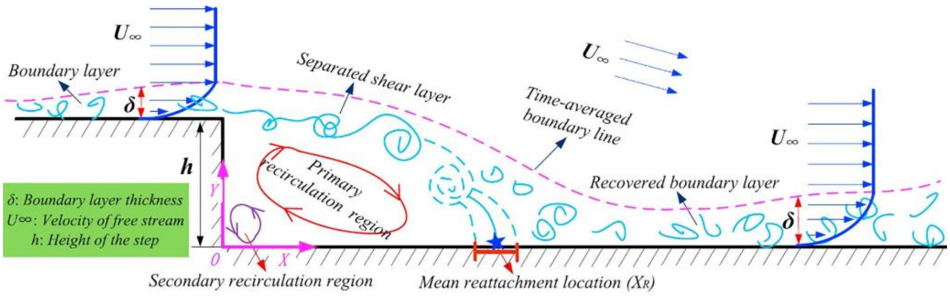

Fig. 1 − Definition of the flow behavior in the BFS stream (Guo *et al*., 2017).

The reason why BFS is preferred especially in thermal applications with high-performance heat exchangers is that flow separation and reattachment perform to improve heat transfer (Kherbeet *et al*., 2016). However, BFS exhibits a low heat transfer due to the recirculation occurring in the region until reattachment, and this weak side has been addressed by many studies (Zdanski *et al*., 2016; Ahmed *et al*., 2018). The degree of inefficacy relies on many factors such as flow regime (laminar or turbulence), thermophysical properties of the fluid, expansion ratio (ER), and expansion angle (α). Many studies have been carried out by researchers to eliminate this disadvantage and provide the highest heat transfer between the flow-surface area in the BFS. When investigating the studies in the literature, it can be mentioned that these techniques are divided into three groups: behind of expansion, point of expansion, and ahead of expansion. These studies generally focused on passive heat transfer enhancement techniques detailed in (Gürsoy *et al*., 2023). Within this scope, subsequent studies have been conducted by researchers before expansion. Cadirci and Gunes, (2014) carried out a numerical investigation on 2D BFS to enhance the heat transfer by preventing the recirculation region behind the BFS. For this purpose, the researchers have inserted an actuator plate. Because of this integration, the intensity of vorticity performed an increment, and heat transfer was enhanced with the help of the vortex formed in the enhanced BFS. Another study has been put forward by Terekhov *et al*., (2022) to examine the effect of obstacles with various sizes and locations on the recirculation region of the BFS. The analyses have been carried out at Reynolds number (Re) of 4000 and it can be mentioned that obstacles greatly affect the local pressure distribution and heat transfer behind the separation. It has been determined that this flow phenomenon increases the maximum heat transfer to the recirculation region and brings it closer to the step side. Dyachenko *et al*., (2015) experimentally investigated the thermal and dynamic characteristics of a BFS with a transverse square prism placed behind of sudden expansion region. The results indicate that the transverse square prism notably increases the heat transfer coefficient behind the sudden expansion. As rising of the prism height, it has been detected that the heat transfer effect gains a more pronounced condition.

The research covers the enhancement of heat transfer and flow characteristics ahead of BFS is a modern issue and many studies have been published for this investigation. For this purpose, Pazarlıoğlu *et al*., (2023) conducted a numerical study on a BFS with elliptical dimpled fins inserted on the ahead sudden expansion region. While the analyses have been investigated for the laminar flow regime (100≤Re≤2000), $CoFe_2O_4/H_2O$ nanofluid has been used as the working fluid. The researchers have made an effort to find the optimal case in the flow geometry by considering the pitch length and dimpled fin direction. It is concluded that the performance evaluation criterion (PEC) of BFS increased by 110% and 10.5% because of the vertical elliptical dimpled fin and $CoFe_2O_4$/water nanofluid, respectively. Gürsoy *et al*., (2022) showed that the convective heat transfer rate through the BFS enhanced with the help of the insertion of spherical dimpled fins and Fe_3O_4/water (ferrofluid) nanofluid. Thanks to the combination of two parameters, the PEC increased by 110%. Another study carried out by Gürsoy *et al*., (2024) performed for not only dimpled fin and nanofluid but also expansion angle. In this study, vertical elliptical dimpled fins and Al_2O_3/water with different nanoparticle shapes, as well as four different expansion angles (α=30, 45, 60, and 90°), have been utilized. Similar to other results in the literature, in this study, the use of dimpled fins and nanofluids resulted in significant findings on the system performance, and the determination that the α=45° expansion angle provided the highest performance presented a special result compared to other studies.

There are seldomly encountered studies that have directly affected the occuring of the sudden expansion flow mechanism have been investigated. Abbassi and Ben Nassrallah, (2007) examined the effect of a magnetic field on the direct recirculation zone. In the numerical analysis, a 2D BFS with ER=2 and a single expansion side has been utilized. Besides, a working fluid, in which the

Prandtl number (Pr) changes from 0.02 to 7.0 (like from liquid metal to water) has been used at Re=100, 200, 300, and 380. It is presented that heat transfer considerably increases with the application of a magnetic field, particularly for high Pr. On the other hand, reattachment length and subsequently recirculation region size decreases with this external magnetic field. Mehrez and El Cafsi, (2019) analyzed the heat transfer and flow characteristics in a BFS with 2D single side expansion. Researchers have used Al_2O_3-Cu/water hybrid nanofluid at $100 \leq Re \leq 300$ and applied magnetic field varies from 0 to 50 Ha on recirculation region. According to the results, reattachment length decreases with increasing hybrid nanofluid volume concentration (φ) and decreasing of Re. Besides, recirculation region size has been damped by increasing magnetic field strength. In heat transfer characteristics, the average Nusselt number (Nu) increases with an increment of φ and magnetic field strength.

Another issue that is outside the scope of geometric or external force is the physical effect of the thermophysical properties of the working fluid during sudden expansion. In this study, it is considered that Fe_3O_4 nanoparticles are added to the water. Besides, it is a known phenomenon that adding nanoparticles increases the viscosity and density of base fluid (Chavan and Pise, 2019). Variation in viscosity and density is directly related to the Coanda effect and this phenomenon is identified as the tendency of a moving fluid to attach itself to a nearby surface and flow along it (Ahmed, 2019). When an increment occurs in the viscosity of the working fluid, high-viscosity fluids tend to exhibit stronger Coanda effects because they adhere more readily to surfaces. Furthermore, an increment occurs in density, working fluid has a more pronounced Coanda effect due to increased momentum transfer (Trancossi, 2011).

Based on the literature research, it is concluded that there are many investigations covering the heat transfer and flow characteristics of BFS particularly in geometric configurations. Besides, most of the studies have been carried out for single-side expanded BFS. However, there are not enough comprehensive studies about the effect of magnetic field and nanofluid volume concentration effect on secondary flow in BFS. In this study, a numerical investigation has been carried out for 3D circular BFS (double-side expanded). As a working fluid, ferrofluid with φ=1.0, 1.5, and 2.0% has been utilized and a constant magnetic field with strength of B=0.3, 0.5, 0.7, and 1.0T has been applied on the sudden expansion region to observe the heat transfer and flow characteristics.

2. Material and Methods

Heat transfer and flow characteristics analysis of 3D circular BFS have been carried out under the laminar flow regime ($500 \leq Re \leq 2000$). The schematic view of the fluid domain has been presented in Fig. 2. The length and diameter of the inlet tube are designated as L_1=375 mm and D_1=8 mm. Working fluid inlets at different velocities, which vary to Re and φ, and constant temperature of T_{in}=300K. Then, the inlet tube connects with the outlet tube with length and diameter are L_2=1125 mm and D_2=20 mm, respectively, and consequently working fluid exposed to double-side expansion. Once the fluid expands, it is exposed to an external constant magnetic field (B=0.3, 0.5, 0.7, and 1.0T) effect along the first section with L=100 mm of the outlet tube. In addition, the working fluid was heated by applying a heat flux of q''=600 W/m^2 to the outlet tube wall. In this way, the effect of the magnetic field boundary condition applied to the fluid on the thermal performance of the system could be examined. It is assumed that the working fluid flows into the environment of P_{out}=1 atm when leaving the system. Besides, the no-slip condition has been considered for entire walls.

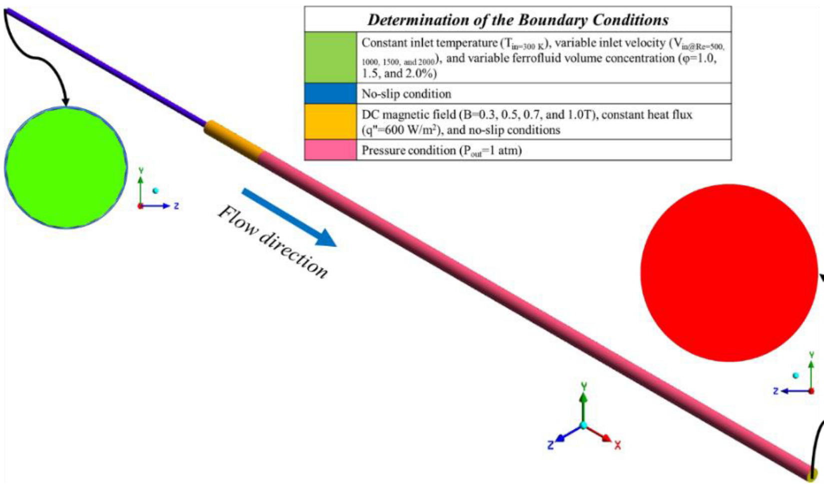

Fig. 2 – Schematic view and boundary condition of the fluid domain.

Ferrofluid with φ=1.0, 1.5, and 2.0% is used as a working fluid. The reason for the selection of the Fe_3O_4 nanoparticle is that it has prominent magnetic properties. Besides, it has been assumed that particles have a spherical shape. Consequently, the thermophysical properties of water and Fe_3O_4 nanoparticles are presented in Table 1.

Table 1

Thermophysical properties of water and Fe_3O_4 nanoparticles (Gürdal *et al.*, 2022)

Matter	Density [kg·m^{-3}]	Specific heat [J·kg^{-1}·K^{-1}]	Thermal conductivity [W·m^{-1}·K^{-1}]	Dynamic viscosity [kg·m^{-1}·s^{-1}]	Electrical conductivity [S·m^{-1}]
Water	*998*	*4182*	*0.6*	*0.001003*	*0.05*
Fe_3O_4	*5180*	*670*	*80.4*		*25000*

In order to calculate the thermophysical properties of ferrofluid, well-known correlations have been utilized. Within the scope of this paper, the density of nanofluid is calculated with Eq. (1) (Bahmani *et al.*, 2018).

$$\rho_{nf} = (1-\varphi)\rho_{bf} + \varphi\rho_{np} \tag{1}$$

where: ρ specifies the density, [kg·m^{-3}], and *nf*, *bf*, and *np* subscripts describe the nanofluid, base fluid, and nanoparticle, respectively. The thermal conductivity of nanofluid can be found in Eq. (2) (Lahmar *et al.*, 2020).

$$\frac{k_{nf}}{k_{bf}} = \frac{k_{np} + 2k_{bf} - 2\varphi\left(k_{bf} + k_{np}\right)}{k_{np} + 2k_{bf} + \varphi\left(k_{bf} + k_{np}\right)} \tag{2}$$

where: k describes the thermal conductivity, [W·m^{-1}·K^{-1}]. Besides, specific heat can be described by Eq. (3) (Adun *et al.*, 2021).

$$c_{p_{nf}} = \frac{(1-\varphi)\left(\rho c_p\right)_{bf} + \varphi\left(\rho c_p\right)_{np}}{\rho_{nf}} \tag{3}$$

where: c_p identifies the specific heat of ferrofluid, [J·kg^{-1}·K^{-1}]. Dynamic viscosity calculated with Eq. (4) (Khodadadi *et al.*, 2018).

$$\mu_{nf} = \left(1 + 7.3\varphi + 123\varphi^2\right)\mu_{bf} \tag{4}$$

where: μ shows the dynamic viscosity of ferrofluid, [kg·m^{-1}·s^{-1}]. Finally, effective electrical conductivity can be defined with Eq. (5) (Sheikholeslami *et al.*, 2015).

$$\frac{\sigma_{nf}}{\sigma_{bf}} = 1 + \frac{3\left(\frac{\sigma_{np}}{\sigma_{bf}} - 1\right)\varphi}{\left(\frac{\sigma_{np}}{\sigma_{bf}} + 2\right) - \left(\frac{\sigma_{np}}{\sigma_{bf}} - 1\right)\varphi} \tag{5}$$

where: σ symbolizes the electrical conductivity of ferrofluid, [S·m^{-1}]. Some equations were used to make the data obtained from the numerical results meaningful from a thermohydraulic perspective. Based on this purpose, Re is calculated with Eq. (6).

$$\mathrm{Re} = \frac{\rho V D}{\mu} \tag{6}$$

where: V and D describe the fluid velocity and inlet tube diameter, [m·s^{-1}], [m], respectively. The convective heat transfer coefficient is described by Eq. (7).

$$h = \frac{q''}{(T_w - T_b)} \tag{7}$$

where: h denotes the convective heat transfer coefficient, [W·m^{-2}·K^{-1}], T_w identifies the average outlet tube wall temperature, [K], and T_b shows the bulk temperature, [K]. The bulk temperature is calculated with the help of Eq. (8).

$$T_b = \frac{T_{in} + T_{out}}{2} \tag{8}$$

where: T_{in} shows the inlet temperature, [K], and T_{out} identifies the outlet temperature, [K]. To present the convective heat transfer rate as dimensionless, the average Nu is considered with the help of Eq. (9).

$$Nu = \frac{hD}{k} \tag{8}$$

Darcy friction factor (ff) calculated with Eq. (10).

$$ff = \frac{\Delta P}{\left(\frac{L}{D}\right)\left(\frac{\rho V^2}{2}\right)} \tag{10}$$

where: ΔP and L show the pressure drop and tube length, [Pa], [m], respectively. To calculate the system performance, the PEC is calculated with the help of Eq. (11).

$$PEC = \frac{Nu_{enhanced} / Nu_{base}}{ff_{enhanced} / ff_{base}} \tag{11}$$

where: $Nu_{enhaced}$ and $ff_{enhanced}$ symbolize the flowing of ferrofluid and the application of DC magnetic field strength while Nu_{base} and ff_{base} determine the flowing of water.

Ferrofluid has been considered as incompressible and analyses have been carried out for steady-state and single-phase flow. Based on these assumptions, the general conversation equations for continuity, momentum, and energy can written as follows for the 3D fluid domain:

Continuity equation (Gürsoy *et al.*, 2024a):

$$\frac{1}{r}\frac{\partial}{\partial r}\left(r\rho V_r\right)+\frac{1}{r}\frac{\partial\left(\rho V_\theta\right)}{\partial\theta}+\frac{\partial\left(\rho V_z\right)}{\partial z}=0 \tag{12}$$

r-direction of momentum equation (Gürsoy *et al.*, 2024a):

$$\begin{aligned}&\overbrace{\rho\left(V_r\frac{\partial V_r}{\partial r}+\frac{V_\theta}{r}\frac{\partial V_r}{\partial\theta}-\frac{V_\theta^2}{r}+V_z\frac{\partial V_r}{\partial z}\right)}^{\text{Convection terms}}=\\ &\underset{\text{Pressure gradient}}{-\frac{\partial P}{\partial r}}+\underset{\text{Body force terms}}{\rho g_r}\\ &\underbrace{+\mu\left(\frac{\partial^2V_r}{\partial r^2}+\frac{1}{r}\frac{\partial V_r}{\partial r}-\frac{V_r}{r^2}+\frac{1}{r^2}\frac{\partial^2V_r}{\partial\theta^2}-\frac{2}{r^2}\frac{\partial^2V_\theta}{\partial\theta}+\frac{\partial^2V_r}{\partial z^2}\right)}_{\text{Diffusion terms}}\\ &\underbrace{+q\left(E_0+V_rB_0\right)B_0}_{\text{Lorentz force terms}}\end{aligned} \tag{13}$$

where: P shows the pressure, [Pa], g specifies the gravity, [m· s^{-2}], q identifies the electric charge, [C], E describes the electric field, [V/m], and B shows the magnetic field, [T].

θ-direction of momentum equation (Gürsoy *et al.*, 2024a):

$$\overbrace{\rho\left(V_r\frac{\partial V_\theta}{\partial r}+\frac{V_\theta}{r}\frac{\partial V_\theta}{\partial \theta}-\frac{V_rV_\theta}{r}+V_z\frac{\partial V_\theta}{\partial z}\right)}^{\text{Convection terms}}=$$
$$\underbrace{-\frac{1}{r}\frac{\partial P}{\partial \theta}}_{\text{Pressure gradient}}+\underbrace{\rho g_\theta}_{\text{Body force terms}}$$
$$+\underbrace{\mu\left(\frac{\partial^2 V_\theta}{\partial r^2}+\frac{1}{r}\frac{\partial V_\theta}{\partial r}-\frac{V_\theta}{r^2}+\frac{1}{r^2}\frac{\partial^2 V_\theta}{\partial \theta^2}+\frac{2}{r^2}\frac{\partial V_r}{\partial \theta}+\frac{\partial^2 V_\theta}{\partial z^2}\right)}_{\text{Diffusion terms}}$$
$$+\underbrace{q\left(E_0+V_\theta B_0\right)B_0}_{\text{Lorentz force terms}} \tag{14}$$

z-direction of momentum equation (Gürsoy *et al.*, 2024a):

$$\overbrace{\rho\left(V_r\frac{\partial V_z}{\partial r}+\frac{V_\theta}{r}\frac{\partial V_z}{\partial \theta}+V_z\frac{\partial V_\theta}{\partial z}\right)}^{\text{Convection terms}}=\overbrace{-\frac{\partial P}{\partial z}}^{\text{Pressure gradient}}+\overbrace{\rho g_z}^{\text{Body force terms}}$$
$$+\overbrace{\mu\left(\frac{\partial^2 V_z}{\partial r^2}+\frac{1}{r}\frac{\partial V_z}{\partial r}+\frac{1}{r^2}\frac{\partial^2 V_z}{\partial \theta^2}+\frac{\partial^2 V_z}{\partial z^2}\right)}^{\text{Diffusion terms}}\underbrace{+q\left(E_0+V_zB_0\right)B_0}_{\text{Lorentz force terms}} \tag{15}$$

Energy equation (Gürsoy *et al.*, 2024a):

$$\rho c_v\left(V_r\frac{\partial T}{\partial r}+\frac{V_\theta}{r}\frac{\partial T}{\partial \theta}+V_z\frac{\partial T}{\partial z}\right)=$$
$$k\left(\frac{\partial^2 T}{\partial r^2}+\frac{1}{r}\frac{\partial T}{\partial r}+\frac{1}{r^2}\frac{\partial^2 T}{\partial \theta^2}+\frac{\partial^2 T}{\partial z^2}\right)+\mu\Phi+\frac{1}{\sigma}jj \tag{16}$$

where: T specifies the temperature, [K], Φ describes the dissipation energy, [W· m^{-3}], and j symbolizes the current density, [A· m^{-2}].

ANSYS Fluent 2023 R1 commercial program has been used to conduct the analyses (Canonsburg, 2018) software. By means of this software, the required governing equations given in Eq. (12)-(16) have been systematically solved. The solution of governing equations was used in the setup section. In this case, the SIMPLE scheme was used as Pressure-Velocity Coupling to enable faster iteration than PISO and COUPLED algorithms, impress the continuity, and correlate between velocity and pressure corrections obtaining a pressure gradient. Moreover, within the SIMPLE algorithm, the utilization of under-relaxation for adjusting the pressure correction value, denoted as p', presents a notable strategy. However, determining the appropriate relaxation factor poses a considerable challenge. The under-relaxation approach serves to inhibit the simultaneous updating of both the velocity and pressure fields, thereby influencing the convergence rate over time (Wang *et al.*, 2018). Besides, the Second Order Scheme has been preferred to correct pressure results, while Least Squares Cell-Based and Second Order Upwind methods have been selected in Spatial Discretization in gradient, pressure, and momentum solutions. The residual limit values for continuity and velocities have been set up as 10^{-4}, while energy and UDS values have been considered as 10^{-6}.

The analysis method in this software is based on the finite volume method and consequently, the fluid domain has been divided into small volumes to carry out the solution of governing equations. The most important issues in this step are the optimization of mesh element number and the forming of mesh structure considering the mesh quality metrics limit values. Within the scope of this paper, the fluid domain has been meshed with the help of local and global mesh settings and the inflation layers have been formed in order to obtain a better solution in the near-wall region. To determine the independency of the numerical results arising from element number, a mesh convergence analysis has been carried out based on the average Nu and ff for approximately constant mesh quality metrics at Re=2000 considering water flow. After the element number 1309107, the results have gained stability as given in Fig. 3. The mesh structure belonging to the convergence study is given in Fig. 4.

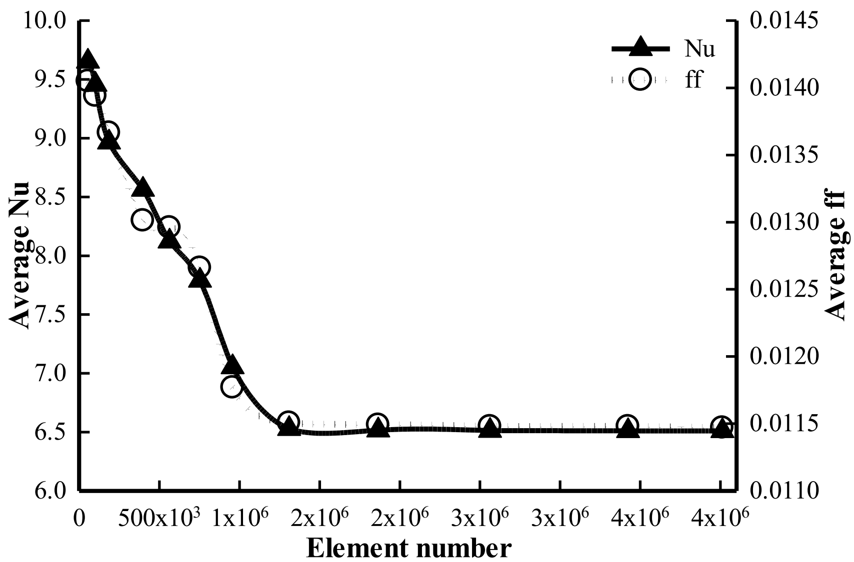

Fig. 3 – Mesh convergence study results.

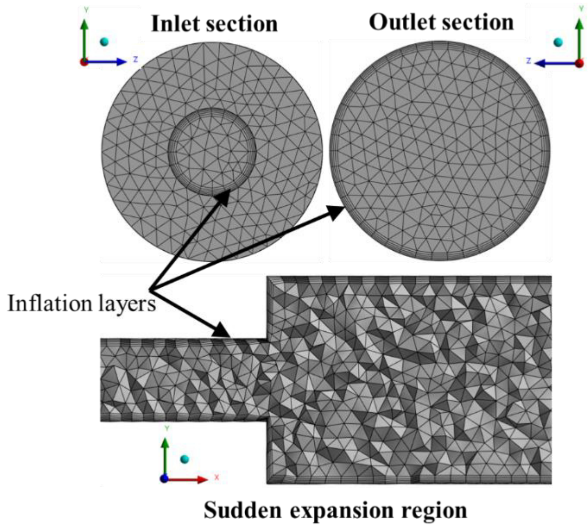

Fig. 4 – Fluid domain mesh structure.

The last step before parametric analysis is to validate the results based on the applied solution method and formed mesh structure. For this purpose, validation has been conducted with average ff results for water at Re=2000 and a comparison has been done with the study of Pazarlıoğlu *et al*., (2023). The results presented a high harmony with each other as can be seen in Fig. 5 and the average error rate was acquired as 2.33%.

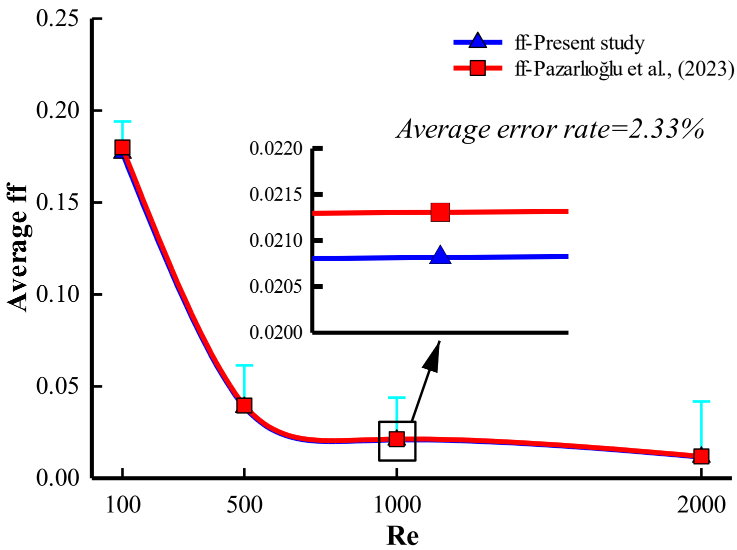

Fig. 5 – Validation of the numerical results study results.

3. Results and Discussion

Firstly, the volume concentration effect of ferrofluid is discussed in Fig. 6. It is seen that φ=1.0% performed the highest average Nu, and increasing the Re enhanced the convective heat transfer rate in the system. In addition, increasing φ leaves a negative mark on the thermal system. Compared with water at Re=2000, φ=1.0% enhanced the heat transfer by about 2.5% whereas φ=1.5 and 2.0% decreased it. The reason for this situation is explained by Vafaei *et al.*, (2021) as follows: if energy transfer between fluid layers becomes dominant with increasing nanofluid viscosity, convective heat transfer decreases with nanoparticle concentration. From this result, it can be seen that the viscosity increase of the ferrofluid examined within the scope of the study dominates. It has been also concluded that the increasing of φ negatively affects the average f in the tube as aspected. This is another effect of increasing viscosity and is a result of decreased fluid movement (Hussein *et al.*, 2013). In this study, the average f of ferrofluid with φ=1.0, 1.5, and 2.0% caused an increment by 0.79%, 1.72%, and 3.24% at Re=2000 compared with water. On the other hand, Fig. 7 presents the local Nu and velocity streamlines at Re=500 on the sudden expansion region. According to the color distribution in Fig. 7(a), φ=1.0% slightly performed more convective heat transfer than other concentrations. The reason for more convective heat transfer in certain regions is inherently realized in the studied geometry because of reattachment phenomena (Xie and Xi, 2017). There is no any discrepancy between the velocity streamlines based on the φ variation and the region where reattachment took place has not changed.

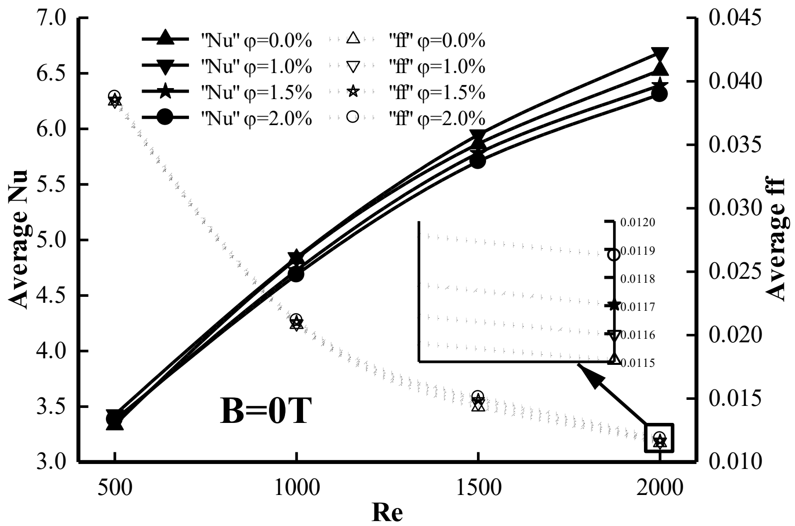

Fig. 6 – Variation of the average Nu and ff as Re function under B=0T.

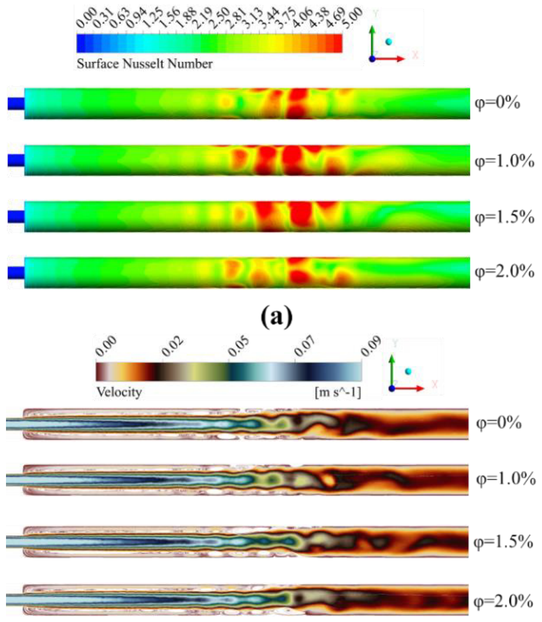

Fig. 7 – Visual comparison of ferrofluid volume concentration on sudden expansion region at Re=500; (a) local Nu variation and (b) velocity streamlines.

As a result of this thermo-hydraulic characteristic examination, the PEC results rely on the variation of φ is presented in Fig. 8. Among the ferrofluid concentrations, φ=1.0% is the only concentration that provided the highest PEC and it performed an increment by 2.66% at Re=500 compared with water.

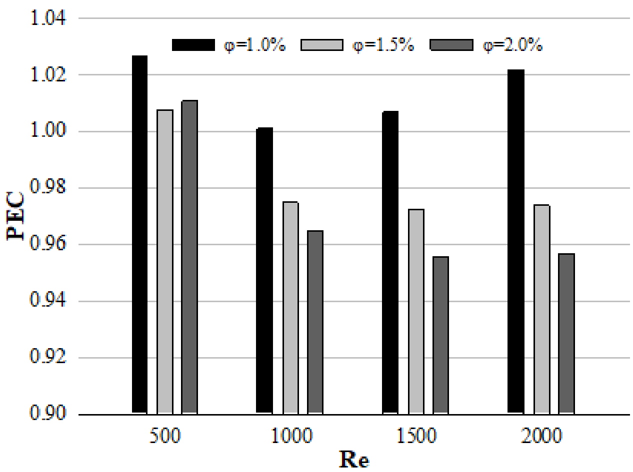

Fig. 8 – Variation of the PEC as Re function under B=0T.

The average Nu and ff variation with Re and B are displayed in Fig. 9. In order to present the magnetic field effect, ferrofluid concentration is selected as φ=1.0% because of performed the highest PEC. From the relevant figure, it can be seen that as the constant magnetic field strength increases, the average Nu increases, significantly. The factor that causes this situation is the Lorenz force, which creates resistance to flow under the influence of the magnetic field of the electrically charged nanoparticles that make up ferrofluid. Thanks to this force, vortex formation in the flow is observed, which activates the boundary layers and increases convective heat transfer (Shah *et al.*, 2021). It has been determined that as the magnetic field strength increases, the average Nu value compared to B=0T tends to occur at the lowest Re value. Compared with the average Nu of B=0T at Re=500, an increase in the rate of 31.5%, 91.6%, 102.0%, and 117.7% at B=0.3, 0.5, 0.7, and 1.0T were calculated, respectively.

However, the effect of this formation on friction is considerable. As can be seen from Fig. 9, significant increases in ff occurred due to the Lorentz forces, which have a positive effect on convective heat transfer, forming resistance to flow. Compared with the average ff of B=0T at Re=500, an increase in the rate of 53.54%, 121.46%, 202.89%, and 343.89% at B=0.3, 0.5, 0.7, and 1.0T were calculated, respectively.

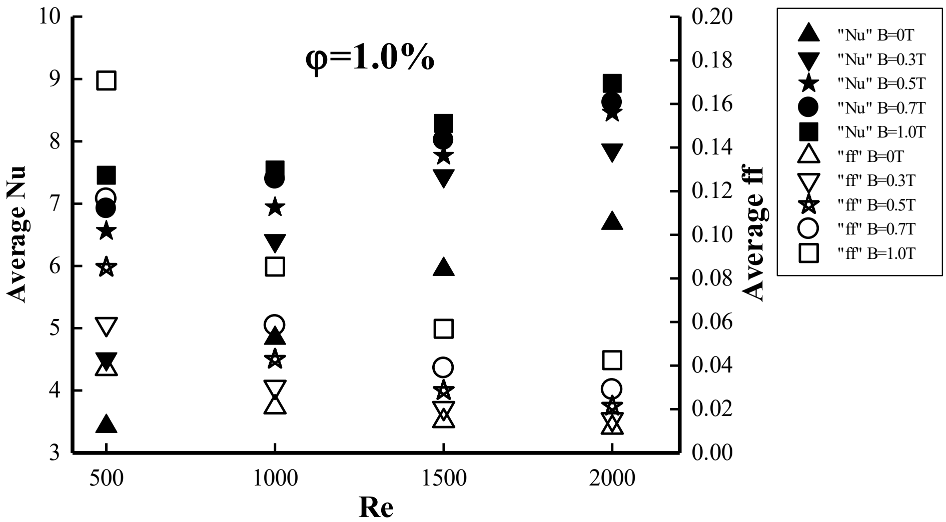

Fig. 9 – Variation of the average Nu and ff as Re function under different B for φ=1.0%.

The thermo-hydraulic characteristics results presented polyvalent information about the effect of magnetic fields on the system performance. When Fig. 11 is examined, it is concluded that PEC tends to decrease after B=0.5T and that the optimum conditions for BFS within the scope of this study are ferrofluid flow including φ=1.0% at B=0.5T. Another finding that should be underlined is that PEC tends to decrease as Re increases. According to the calculations, B=0.3, 0.5, 0.7, and 1.0T increase the PEC at the rate of 14.0%, 47.0%, 39.7%, and 32.4%, respectively, compared with B=0T at Re=500.

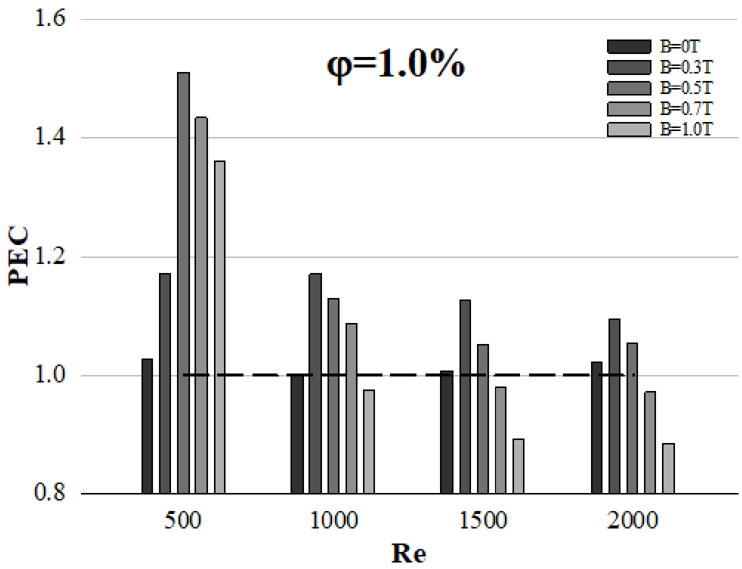

Fig. 10 – Variation of the PEC as Re function under different B for φ=1.0%.

A visual description of the magnetic field effect is presented in Fig. 11, and it is certainly mentioned that the magnetic field considerably changes the BFS flow characterization. As a result of this, well-known phenomena such as reattachment and primary recirculation regions lose their effect. As can be seen in local Nu and velocity streamlines around the sudden expansion region, the reattachment phenomenon is clearly seen for B=0T. However, applying of magnetic field affects the flow mechanism in BFS and restricts the primary recirculation region. Furthermore, the reattachment phenomenon disappeared and the effect of the magnetic field on flow characteristics is significantly affected by increasing of B. Because of the presence of the magnetic field, the convective heat transfer rate in the primary recirculation region enhanced and this results positively affect the thermal performance of BFS based on the PEC.

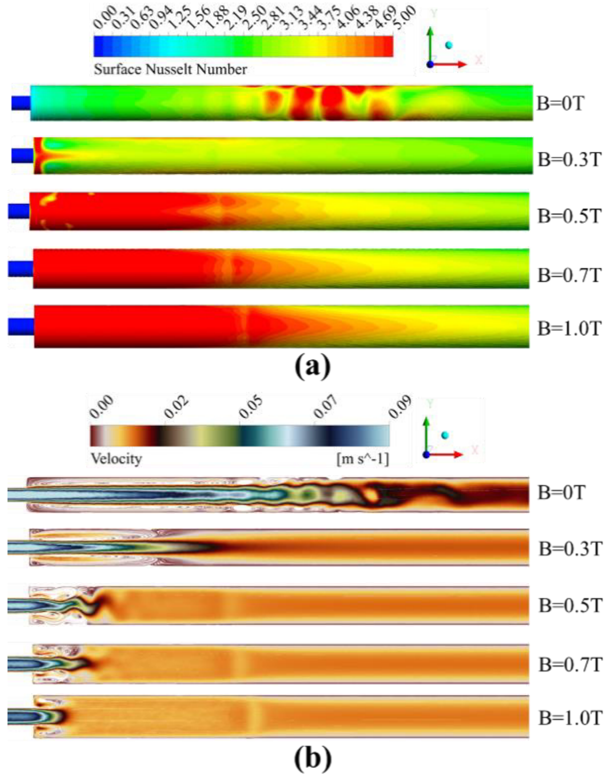

Fig. 11 – Visual comparison of magnetic field on sudden expansion region at Re=500; (a) local Nu variation and (b) velocity streamlines.

3. Conclusions

In this study, heat transfer and flow mechanism of a 3D circular cross-section BFS under constant magnetic field effects (B=0.3, 0.5, 0.7, and 1.0T) and ferrofluid (φ=1.0, 1.5, and 2.0) flows were numerically investigated for laminar flow condition (Re=500, 1000, 1500, and 2000). The governing equations for this geometry were solved considering the incompressible and steady-state flow using ANSYS Fluent 2023R1. The significant attained results in the research are presented in the following:

- Although it is a known fact that thermal conductivity increases as the nanofluid concentration increases, in this study the highest average Nu was obtained at φ=1.0% due to the more dominant effect of ferrofluid viscosity on the boundary layers. Ferrofluid with φ=1.0% increased the average Nu at the rate of 2.5% at Re=2000.

• It was determined that as the ferrofluid concentration increases, the ff also increases and accordingly the highest PEC occurs at φ=1.0%. The increment rate is acquired as 2.66% for PEC at Re=500.

• It has been found that as the magnetic field strength increases, the average Nu value at B=0T tends to be lowest at the smallest Re value.

• Compared to the average Nu at B=0T and Re=500, the increases were 31.5%, 91.6%, 102.0%, and 117.7% at magnetic field strengths of 0.3T, 0.5T, 0.7T, and 1.0T, respectively.

• Increasing the magnetic field strength negatively impacted the system's PEC, as it led to a higher friction coefficient. A decrease in system performance was observed when the magnetic field strength exceeded 0.5T.

• It was concluded that B=0.5T at Re=500 increased PEC by 47%.

• It has been observed that as the magnetic field strength increases, the reattachment phenomenon in the BFS disappears.

• Magnetic field strength and nanofluid concentrations are a key parameters for flow control applications on the BFS. Optimized these parameters can lead further improvement in thermal systems' performance.

REFERENCES

Abbassi H., Nassrallah S. Ben, *MHD flow and heat transfer in a backward-facing step*, Int. Commun. Heat Mass Transf. 34:231–237 (2007), doi:10.1016/J.ICHEATMASSTRANSFER.2006.09.010.

Adun H., Wole-Osho I., Okonkwo E.C., Kavaz D., Dagbasi M., *A critical review of specific heat capacity of hybrid nanofluids for thermal energy applications*, J. Mol. Liq. 340:116890 (2021), doi:10.1016/J.MOLLIQ.2021.116890.

Ahmed H.E., Kherbeet A.S., Ahmed M.I., Salman B.H., *Heat transfer enhancement of micro-scale backward-facing step channel by using turbulators*, Int. J. Heat Mass Transf. 126: 963–973 (2018), doi:10.1016/J.IJHEATMASSTRANSFER.2018.05.082.

Ahmed N.A., *Coanda Effect: Flow Phenomenon and Applications*, CRC Press (2019).

Bahmani M.H., Sheikhzadeh G., Zarringhalam M., Akbari O.A., Alrashed A.A.A.A., Shabani G.A.S., Goodarzi M., *Investigation of turbulent heat transfer and nanofluid flow in a double pipe heat exchanger*, Adv. Powder Technol. 29:273–282 (2018), doi:10.1016/J.APT.2017.11.013.

Cadirci S., Gunes H., *Heat Transfer Enhancement Behind a Backward Facing Step with Active Flow Control*, J. Therm. Sci. Technol. Bilim. ve Tek. Derg. 34 (2014).

Canonsburg A.D., *ANSYS Fluent User ' s Guide* (2018).

Chavan D., Pise A., *Experimental Investigation of Effective Viscosity and Density of Nanofluids*, Mater. Today Proc. 16:504–515 (2019), doi:10.1016/J.MATPR.2019.05.122.

Chen L., Asai K., Nonomura T., Xi G., Liu T., *A review of Backward-Facing Step (BFS) flow mechanisms, heat transfer and control*, Therm. Sci. Eng. Prog. 6:194–216 (2018), doi:10.1016/J.TSEP.2018.04.004.

Dyachenko A.Y., Smul'sky Y.I., Terekhov V.I., Yarygina N.I., *Turbulent mixing of small-obstacle-induced perturbations with the separated shear layer behind a backward-facing step*, Thermophys. Aeromechanics 22:677–688 (2015).

Guo G. Ming, Liu H., Zhang B., *Numerical study of active flow control over a hypersonic backward-facing step using supersonic jet in near space*, Acta Astronaut. 132:256–267 (2017), doi:10.1016/J.ACTAASTRO.2016.12.035.

Gürdal M., Pazarlıoğlu H.K., Tekir M., Arslan K., Gedik E., *Numerical investigation on turbulent flow and heat transfer characteristics of ferro-nanofluid flowing in dimpled tube under magnetic field effect*, Appl. Therm. Eng. 200:117655 (2022), doi:10.1016/J.APPLTHERMALENG.2021.117655.

Gürsoy E., Kadir Pazarlıoğlu H., Dağdeviren A., Gürdal M., Gedik E., Arslan K., Kurt H., *Energy analysis of magnetite nanofluid flowing in newly designed sudden expansion tube retrofitted with dimpled fin*, Int. J. Heat Mass Transf. 199:123446 (2022), doi:10.1016/J.IJHEATMASSTRANSFER.2022.123446.

Gürsoy E., Pazarlioğlu H.K., Gürdal M., Gedik E., Arslan K., Dağdeviren A., *Investigation of magneto-convection characteristics in a sudden Expanding Channel with convex surface geometry under thermally developing flow conditions*, Int. J. Numer. Methods Heat Fluid Flow (2024a).

Gürsoy E., Pazarlıoğlu H.K., Gürdal M., Gedik E., Arslan K., *Entropy generation of ferronanofluid flow in industrially designed bended dimpled tube*, Therm. Sci. Eng. Prog. 37:101620 (2023), doi:10.1016/J.TSEP.2022.101620.

Gürsoy E., Pazarlıoğlu H.K., Gürdal M., Gedik E., Arslan K., *Parametric analysis of different Al2O3 nanoparticle shapes and expansion angles for sudden expanded tube regarding the first law of thermodynamics*, Int. J. Therm. Sci. 197:108759 (2024b), doi:10.1016/J.IJTHERMALSCI.2023.108759.

Hussein A.M., Sharma K.V., Bakar R.A., Kadirgama K., *The effect of nanofluid volume concentration on heat transfer and friction factor inside a horizontal tube*, J. Nanomater, 2013:1–12 (2013).

Kherbeet A.S., Safaei M.R., Mohammed H.A., Salman B.H., Ahmed H.E., Alawi O.A., Al-Asadi M.T., *Heat transfer and fluid flow over microscale backward and forward facing step: A review*, Int. Commun. Heat Mass Transf. 76:237–244, (2016), doi:10.1016/J.ICHEATMASSTRANSFER.2016.05.022.

Khodadadi H., Aghakhani S., Majd H., Kalbasi R., Wongwises S., Afrand M., *A comprehensive review on rheological behavior of mono and hybrid nanofluids: Effective parameters and predictive correlations*, Int. J. Heat Mass Transf. 127:997–1012 (2018), doi:10.1016/J.IJHEATMASSTRANSFER.2018.07.103.

Lahmar S., Kezzar M., Eid M.R., Sari M.R., *Heat transfer of squeezing unsteady nanofluid flow under the effects of an inclined magnetic field and variable thermal conductivity*, Phys. A Stat. Mech. its Appl. 540:123138 (2020), doi:10.1016/J.PHYSA.2019.123138.

Mehrez Z., El Cafsi A., *Forced convection magnetohydrodynamic Al2O3–Cu/water hybrid nanofluid flow over a backward-facing step*, J. Therm. Anal. Calorim. 135:1417–1427 (2019), doi:10.1007/s10973-018-7541-z.

Pazarlıoğlu H.K., Gürsoy E., Gürdal M., Tekir M., Gedik E., Arslan K., Taşkesen E., *The first and second law analyses of thermodynamics for CoFe2O4/H2O flow in a sudden expansion tube inserted elliptical dimpled fins*, Int. J. Mech. Sci. 246:108144 (2023), doi:10.1016/J.IJMECSCI.2023.108144.

Shah Z., Ikramullah P. Kumam, Selim M.M., Alshehri A., *Impact of nanoparticles shape and radiation on the behavior of nanofluid under the Lorentz forces*, Case Stud. Therm. Eng. 26:101161 (2021), doi:10.1016/J.CSITE.2021.101161.

Sheikholeslami M., Rashidi M.M., Ganji D.D., *Effect of non-uniform magnetic field on forced convection heat transfer of Fe3O4–water nanofluid*, Comput. Methods Appl. Mech. Eng. 294:299–312 (2015), doi:10.1016/J.CMA.2015.06.010.

Terekhov V.I., Dyachenko A.Y., Smulsky Y.J., Sunden B., *Intensification of heat transfer behind the backward-facing step using tabs*, Therm. Sci. Eng. Prog. 35:101475 (2022), doi:10.1016/J.TSEP.2022.101475.

Trancossi M., *An overview of scientific and technical literature on Coanda effect applied to nozzles*, SAE Int. (2011), doi:doi:10.4271/2011-01-2591.

Vafaei S., Yeager J.A., Daluga P., Scherer B., *Forced convection nanofluid heat transfer as a function of distance in microchannels*, Materials (Basel), 14:3021 (2021).

Wang H., Wang H., Gao F., Zhou P., Zhai Z. (John), *Literature review on pressure–velocity decoupling algorithms applied to built-environment CFD simulation*, Build. Environ. 143:671–678 (2018), doi:10.1016/J.BUILDENV.2018.07.046.

Xie W.A., Xi G.N., *Fluid flow and heat transfer characteristics of separation and reattachment flow over a backward-facing step*, Int. J. Refrig. 74:177–189 (2017), doi:10.1016/J.IJREFRIG.2016.10.006.

Zdanski P.S.B., Vaz Jr M., Gargioni G.T., *Convection heat transfer enhancement on recirculating flows in a backward facing step: The effects of a small square turbulence promoter*, Heat Transf. Eng. 37:162–171 (2016).

STUDIUL TRANSFERULUI DE CĂLDURĂ ȘI A CURGERII UNUI FEROFLUID ÎNTR-UN CILINDRU CU VARIAȚIE TIP TREAPTĂ A RAZEI, CONSIDERÂND INFLUENȚA UNUI CÂMP MAGNETIC EXTERIOR

(Rezumat)

Etapa de curgere în sens invers este critică în aplicațiile de transfer de căldură, în special în sistemele de încălzire și răcire, datorită fenomenelor sale reologice unice, cum ar fi reatașarea și separarea fluxului. Raportul de expansiune, unghiul, regimul de curgere și proprietățile termofizice ale fluidului de lucru influenţează semnificativ mecanismele de transfer și de curgere a căldurii. Studiul numeric a fost realizat pe o treaptă cu secțiune transversală circulară orientată înapoi, cu un raport de expansiune de 2,5 și unghi de 90°. S-a utilizat un ferofluid magnetizabil cu concentrații de volum de φ=1,0, 1,5 și 2,0% în regimuri de curgere laminară ($50 \leqslant Re \leqslant 2000$), expus la un câmp magnetic uniform (B=0,3, 0,5, 0,7 și 1,0T) și încălzit la un flux constant de q"=600 W/m^2. Rezultatele au arătat că ferofluidul cu φ=1,0% a avut cel mai mare număr Nusselt și performanță maximă. În plus, creșterea intensității câmpului magnetic nu numai că

îmbunătățește transferul de căldură convectiv, ci determină și reducerea acestuia. Câmpul magnetic a influențat semnificativ reatașarea și recircularea, iar cazul optim este obținut pentru B=0,5T la Re=500.)